


Article

Effect of High Temperature Reconstruction and Modification on Phase Composition and Structure of Steel Slag

Shuai Hao, Guoping Luo *, Yuanyuan Lu, Shengli An , Yifan Chai and Wei Song

School of Materials and Metallurgy, Inner Mongolia University of Science and Technology, Baotou 014010, China

* Correspondence: luoguoping3@126.com

Abstract: This study investigates the pattern of influence of blast furnace slag tempering on the composition and structure of steel slag. The chemical composition, equilibrium phase composition, microscopic morphological characteristics and elemental composition of microscopic regions of steel slag and blast furnace slag modified by high temperature reconstruction were analyzed using X-ray diffractometer (XRD), FactSage7.1 thermodynamic analysis software, mineral phase microscopy and field emission scanning electron microscopy. The results show that blast furnace slag blending can promote the generation of a low melting point phase in the slag, as well as reducing its melting temperature and improving its high temperature kinetic conditions. On the one hand, the incorporation of blast furnace slag was found to promote the generation of C_2S in the steel slag and improve its gelling activity. Notably, at 1400 °C, the C_2S content (mass fraction) of steel slag modified with 15% high temperature reconstruction reached 39.04%, while that of unmodified steel slag at this temperature was only 16.92%, i.e., only 1/4 of the C_2S content in the modified slag. On the other hand, the incorporation of blast furnace slag inhibited the generation of $a-C_2S-C_3P$ and calcium ferrate minerals, refined the grains of calcium–aluminum yellow feldspar, reduced the alkalinity and promoted the generation of silicate phases with high hydration activity in steel slag.

Keywords: high temperature reconfiguration; steel slag; thermodynamic calculations; gelling activity; X-ray diffractometer



Citation: Hao, S.; Luo, G.; Lu, Y.; An, S.; Chai, Y.; Song, W. Effect of High Temperature Reconstruction and Modification on Phase Composition and Structure of Steel Slag. *Minerals* **2023**, *13*, 67. <https://doi.org/10.3390/min13010067>

Academic Editors: Daniela Guglietta, Stefano Milia, Giovanna Cappai and Adalgisa Scotti

Received: 24 November 2022

Revised: 22 December 2022

Accepted: 28 December 2022

Published: 30 December 2022



Copyright: © 2022 by the authors. Licensee MDPI, Basel, Switzerland. This article is an open access article distributed under the terms and conditions of the Creative Commons Attribution (CC BY) license (<https://creativecommons.org/licenses/by/4.0/>).

1. Introduction

Steel slag, as a by-product of the high temperature steelmaking process, has a chemical composition and mineralogical composition very similar to those of cement and concrete admixtures [1]. However, the low content of cementitious active phase [2], poor stability [3] and high crushing cost of steel slag have become major factors limiting the scale of its use in blending and construction [4]. Therefore, at present, most steel mills still dispose of converter slag in traditional ways, such as piling [5] and landfilling [6–8]. Indeed, the recycling rate is only about 30% [9], which not only presents significant environmental issues [10] but is also a huge waste of resources [11], contributing to the high cost of steel-making.

The temperature of molten steel slag is 1500–1700 °C, and the waste heat quality is high, making it of great value for development and utilization. In the process of steel slag cooling, according to the specific modification requirements, purposely adding modifiers to steel slag to adjust its physical and chemical properties can improve the potential to use this resource. Wang Huigang et al. [12] analyzed the main components of fly ash and their roles in steel slag; the results showed that SiO_2 and Al_2O_3 react with $f-CaO$ to generate stable phases which improve the stability of steel slag while also generating calcium silicate and calcium aluminate. Zhang Xiong [13] studied the carbonation mechanism of zeolite-modified steel slag products. The results showed that after pre-hydration curing for 1 d and carbonation for 2 h, a steel slag test block with 5% zeolite (CSZ5-1 d) had the

best compressive strength, while a steel slag test block with 15% zeolite (CSZ15-1 d) had the best carbonation rate, with increases of 14% and 10.2%, respectively, compared with a pure steel slag test block. Xiang Ruiheng [14] studied preparation and foaming modifications of reconstructed steel slag powder with medium and high activity. It was observed that 75% converter steel slag, 4% bauxite and 21% lime, fired at 1290 °C for 90 min, had the highest C₂S and C₄AF contents after rapid air-cooling, resulting in an increase in water activity to 90.4%, a 2.03% reduction in the *f*-CaO mass fraction, a dissipated RO phase, and increased ease of grinding. It was also demonstrated that the best performance of porous reconstituted steel slag was achieved with a high temperature foaming agent SiC doping content of 1.6%. The activity index of modified steel slag could be increased to 98.2%, and the compressive strength of the composite cement mortar could reach 44.8 MPa. Rao Lei [15] adjusted the alkalinity (2.0~3.0) and Fe₂O₃ content (to about 20%) of a steel slag using quartz sand and coal dust. The results showed that the modified steel slag *f*-CaO mass fraction was reduced by 39.6%, the ease of grinding index was increased by 11% and the 7 d and 28 d activity indices were increased by 3% and 4.8%, respectively. Wang, Chang-Long [16] investigated the high temperature modification of steel slag using reservoir bottom sludge and electroslag stone. The results showed that the 28 d activity index reached 82.4%, with *f*-CaO and *f*-MgO mass fractions of 1.21% and 1.98%, respectively, when the compound modifier was dosed at 20% (reservoir bottom sludge:electroslag stone ratio of 3:1) and the treatment temperature was 1150 °C, which met the production requirements. Li et al. [17] analyzed the effect of electric furnace slag on the properties of steel slag. The results showed that the former can promote the improvement of coagulation in the latter. Zhang Zuoshun et al. [18] investigated the effect of iron tailings on the properties of high temperature steel slag. The results showed that iron tailings can enhance steel slag cementation, while the *f*-CaO content in the steel slag was reduced and its stability was improved. Lei Yunbo et al. [19] studied the effect of fly ash on steel slag in *f*-CaO. The results showed that an admixture of fly ash could reduce the *f*-CaO content in steel slag. Liu Shiye et al. [20] studied the effect of blast furnace slag on the physical phase in steel slag. The results obtained using a 10% blast furnace slag modified steel slag showed that at 1550 °C, the mass fraction of C₂S and C₃S increased significantly, *f*-CaO decreased to 1.64% and the stability improved. In addition, coke reduced the iron in the slag and improved the ease of grinding.

Most of the above research applied pure reagents or reducing agents for steel slag reduction modification treatments. Although the findings were striking, most of the treatment methods would be expensive, precluding their use on an industrial scale. Blast furnace slag is an abundant solid waste resource. Its binary alkalinity ($R=CaO/SiO_2$) is around 1.0, and it has a high content of Al₂O₃, which can be used as a modifier to effectively reduce the alkalinity and stimulate the activity of steel slag, thereby also achieving the goal of “treating waste with waste”. However, few experimental studies have been carried out on the modification of steel slag by high temperature melting using blast furnace slag addition, and the phase composition and structure of steel slag modified by blast furnace slag are not clear. In this paper, under the premise of the “comprehensive utilization of solid waste”, we propose the use of water-quenched blast furnace slag to adjust the alkalinity and physical composition, eliminate the unstable factor and improve the gelation activity of steel slag. This research provides a theoretical basis and experimental data for the modification of steel slag using blast furnace slag.

2. Materials and Methods

2.1. Experimental Materials

In this experiment, water-quenched blast furnace slag and hot-spoiled steel slag were used as raw materials; their chemical compositions are shown in Table 1.

Table 1. Slag proportion and chemical composition (mass fraction, %).

Material	Alkalinity (R)	w(CaO)	w(SiO ₂)	w(Al ₂ O ₃)	w(MgO)	w(Fe ₂ O ₃)	w(FeO)	w(P ₂ O ₅)	w(MnO)
Steel slag	3.27	41.05	12.56	3.11	6.89	15.31	16.44	1.43	3.22
Blast furnace slag	1.30	43.87	33.69	14.88	8.83	1.75	—	—	0.36

Note: Sr-0-Sr-15 are steel slag and modified slag blended with 8, 10, 12 and 15% blast furnace slag, respectively. Alkalinity: Binary alkalinity is used in this paper, i.e., $R = \text{CaO/SiO}_2$.

2.2. Parameters of FactSage7.1

The Equilib module in FactSage7.1 was used to calculate the phase composition of 100 g slag at equilibrium under different temperature conditions and to analyze variations in its phase composition. The specific parameters applied are shown in Table 2.

Table 2. Parameters setting of FactSage7.1.

Database	FToxid7.1、FactPS7.1
Compound type	Monoxide
Solid solution	FToxide-SLAGA、FToxide-SPANNA、FToxide-MeO-A、 FToxide-cPyrA、FToxide-oPyr、FToxide-pPyrA、 FToxide-LcPy、FToxide-WOLLA、FToxide-bC ₂ S、 FToxide-aC ₂ S、FToxide-Mel、FToxide-OlivA

2.3. Experimental Protocol

(1) The steel slag and blast furnace slag were crushed using a crusher and screened using a mesh sieve (0.074 mm). According to the chemical composition and ratio shown in Table 1, blast furnace slag modulated steel slag was made. This was then loaded into the mixing tank on a mixing machine and mixed for 2 h before being taken out for use.

(2) We then placed the slag sample in a molybdenum crucible and put it into a KTF-1700-VT high-temperature vertical furnace. The temperature was ramped up at 10 °C/min from room temperature to 1000 °C, and then from 1000 °C to 1550 °C at a rate of 5 °C/min, holding at that temperature for 1 h. Subsequently, the sample was taken out for emergency water cooling. The whole process took place under an atmosphere of argon gas.

(3) An appropriate amount of roasted specimen was ground to achieve particle sizes of below 0.074 mm, and a composition analysis was carried out using a D8-advanced X-ray diffractometer with a Cu-K α target, with a scanning range of 20°–80° and a scanning speed of 2°/min.

(4) Block specimens were taken. Their surface was first roughly ground and then finely ground and polished. Next, the microscopic morphological characteristics and elemental composition of the microscopic regions were analyzed using a ZEISS ultra-high resolution thermal field emission scanning electron microscope, produced by Zeiss, Germany.

3. Experimental Results and Analysis

3.1. Macrostructure of Modified Slag

The effect of high temperature melting of blast furnace slag modified steel slag after roasting are shown in Figure 1. It can be seen that the surface of the sample became rough with an increase of the proportion of blast furnace slag after roasting, and no crack occurred on the surface. The results show that the fluidity of the modified slag was reduced with an increase of the ratio of blast furnace slag, and that the surface of the synthetic slag was uneven during the cooling process, because the binary basicity of the blast furnace slag was about 1.0 and the fluidity of the low basicity blast furnace slag was poor at high temperature. The surface did not display cracks, indicating that the synthesis did not produce strong internal stresses during the cooling process. It has been shown that the main internal stresses within the steel slag originated from the crystallographic transformation of C₂S and the volume expansion resulting from the hydrolysis of free calcium oxide (*f*-CaO) and free magnesium oxide (*f*-MgO). On the one hand, more pores formed on the surface

of the steel slag not containing blast furnace slag after rapid cooling, while on the other hand, the internal pores became increasingly small for the steel slag mixed with increasing quantities of blast furnace slag. Our analysis indicated that with an increase of the quantity of blast furnace slag, the slag viscosity increased under high temperature conditions and the liquid phase liquidity became poor. Such high viscosity and low liquidity are not conducive to the formation of thin-walled large pore structures, making the internal pores of the slag fine and uneven.

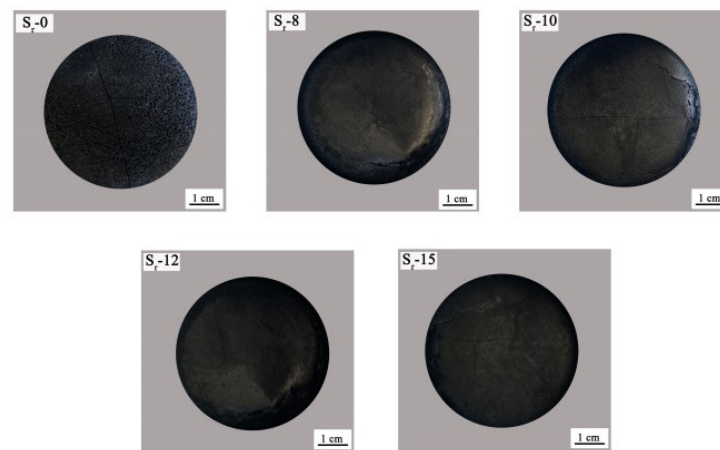


Figure 1. Roasted blast furnace tempered slag specimens.

3.2. Microstructure and Mineral Composition of Modified Slag

Blast furnace slag high-temperature molten modified steel slag roasted specimens were ground and analyzed using an XRD diffractometer (Smartlab, neo-confucianism, Japan) to determine their composition; the results are shown in Figure 2. As shown, the main phases after roasting were C_2AS , C_3AS_3 , $\beta-C_2S$, and C_3S . The main diffraction peak in the XRD diffraction pattern was C_3S , while secondary diffraction peaks were C_3AS_3 and $\beta-C_2S$. With an increase of blast furnace slag doping, the diffraction of the C_3S peak at $2\theta = 35.98^\circ$ showed an overall enhancement. This indicates that the doping of blast furnace slag can promote the generation of C_3S , which does not decompose into C_2S and CaO during rapid cooling; instead, it indirectly reduces the $f-CaO$ content in the slag and improves its stability. At the same time, C_3S has better gelling activity, which enhances the proportion of gelling minerals in steel slag. The C_2AS diffraction peak at $2\theta = 31.18^\circ$ and the diffraction intensity were significantly enhanced in the 15% blast furnace slag doped sample. The intensity of the $\beta-C_2S$ diffraction peak at $2\theta = 33.30^\circ$ did not change significantly, indicating that the doping of blast furnace slag had a small effect on $\beta-C_2S$. C_3AS_3 , an island silicate mineral with a high degree of hardness, showed a diffraction peak at $2\theta = 31.30^\circ$. The generation of large quantities of this compound will increase the cost of steel slag crushing. As observed in the XRD plots, an increase in the blast furnace slag doping ratio enhanced the intensity of the C_3AS_3 diffraction peak in the steel slag. Therefore, it is suggested that the addition of 12% blast furnace slag admixture to steel slag is optimal.

In summary, in the smelting process, the blast furnace slag high temperature molten modified steel slag was fully reacted to form a new phase composition. Blast furnace slag tempering slag can promote the generation of gelling minerals such as C_3S , thereby improving the stability of the steel slag, while blast furnace slag doping resulted in a higher proportion of non-gelling C_2AS and higher hardness C_3AS_3 minerals, indirectly increasing the cost of the subsequent crushing of steel slag. Therefore, in the modification experiments of tempered steel slag, the blast furnace slag admixture percentage was kept below 15%, as this was found to be more conducive to the enhancement of the slag gelling activity [21,22], while the generated C_3S indirectly consumed the $f-CaO$ present in the slag and enhanced its stability.

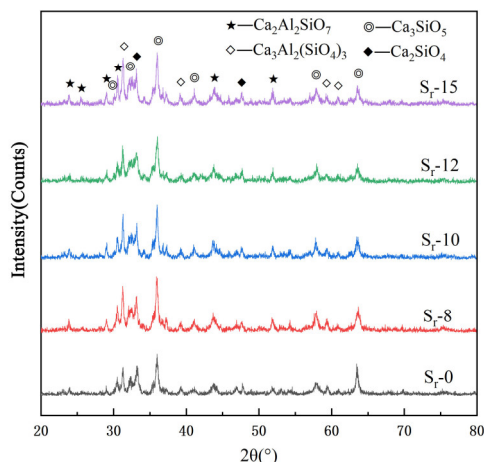


Figure 2. XRD diffraction pattern of blast furnace slag tempered slag roasted specimens.

In order to further confirm the interphase structure relationship of the modified steel slag, the microscopic morphological characteristics and elemental composition of the microscopic regions of the roasted experimental slag specimens were analyzed using mineral microscopy and field emission scanning electron microscopy (sigma300, Zeiss, Germany). The results of the analysis of Sr-0, Sr-8 and Sr-12 into the form hitting points and face sweeping elements are shown in Figures 3–5 and Tables 3–5. From the analysis of the energy spectrum and surface scan in Figure 3 and the elemental distribution in Table 3, the percent elemental content at point 1 in Table 3 was converted into a molar ratio of $n(\text{MgO}):n(\text{FeO}):n(\text{Al}_2\text{O}_3) = 1:1:2$. On these bases, and given the distribution pattern of Mg, Fe, and Al in the vicinity of point 1, as determined by surface sweeping, it is likely that point 1 was an iron-aluminum spinel ($\text{MgO}\cdot\text{FeAl}_2\text{O}_4$, MFA). At point 2 $n(\text{CaO}):n(\text{SiO}_2) = 1.35:0.96:0.17$, and the binding surface sweep was more dispersed in the region, so the silicate phase with phosphorus attached at this point was considered to be $\text{Ca}_3(\text{PO}_4)_2$ and CaSiO_3 . The substance ratio of each oxide at point 3 was about $n(\text{CaO}):n(\text{SiO}_2):n(\text{Al}_2\text{O}_3):n(\text{FeO}) = 4:3:1:1$; a combined surface sweep suggested that calcium-aluminum feldspar mixed with calcium ironate ($\text{Ca}_2\text{Al}_2\text{SiO}_7$, CaFe_2O_4) was present at this point. The material quantity ratio of each oxide at point 4 was roughly as follows: $n(\text{CaO}):n(\text{SiO}_2):n(\text{Al}_2\text{O}_3):n(\text{MgO}):n(\text{MnO}) = 1.8:1.4:0.3:0.3:0.4$. Combined with the location of the ore phase, it was suggested that point 4 was the slag phase, consisting of magnesium aluminum spinel (MgAl_2O_4), calcium silicate (CaSiO_3), and manganese oxide.

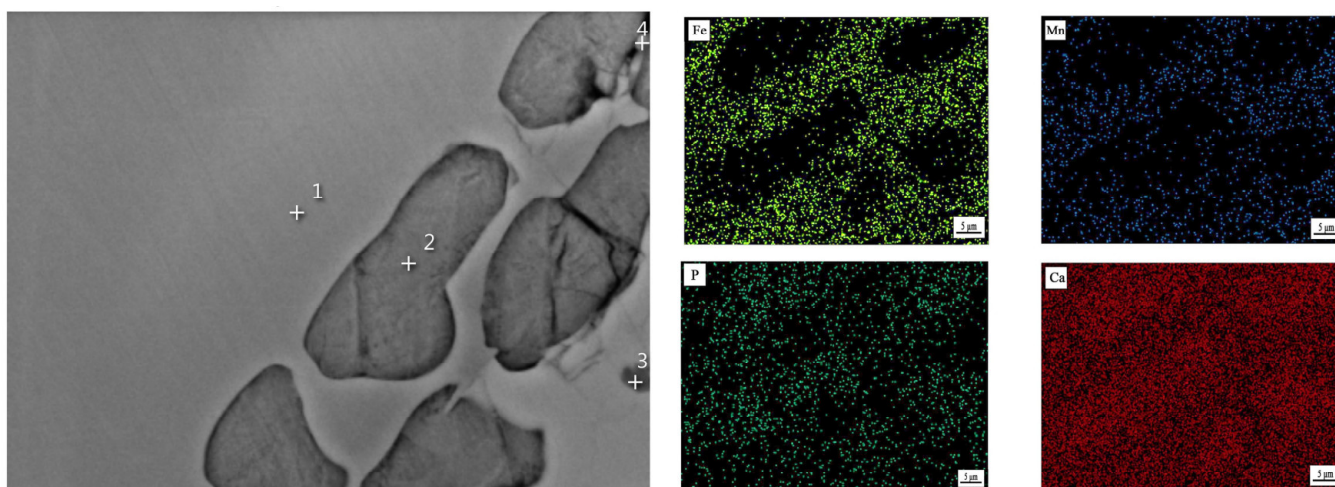


Figure 3. Sr-0 SEM morphology, surface sweep, and energy spectra of four points.

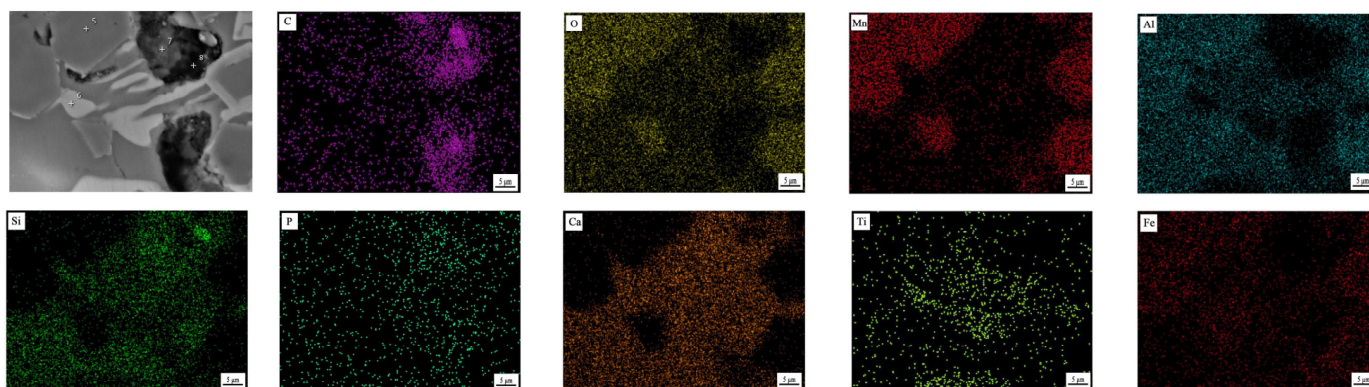


Figure 4. Sr-8 SEM morphology, surface sweep, and point energy spectra.

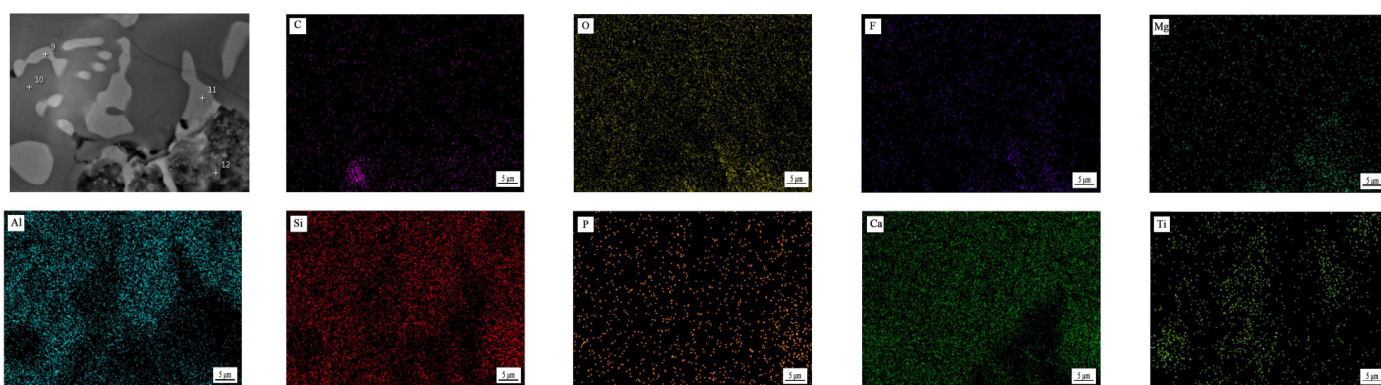


Figure 5. Sr-12 SEM morphology, surface sweep, and energy spectra of points.

Table 3. Sr-0 SEM point element distribution (mass fraction, %).

Element	w(C)	w(O)	w(Mg)	w(Al)	w(Si)	w(P)	w(Ca)	w(V)	w(Ti)	w(Mn)	w(Fe)
Point 1	2.79	40.16	13.44	14.54	0.16	0	0.63	—	—	5.14	23.13
Point 2	4.75	38.96	0.06	0.21	12.57	2.12	38.84	1.11	—	0.33	1.06
Point 3	2.87	34.44	0.41	10.75	3.61	0.11	30.26	—	2.75	2.41	12.39
Point 4	7.62	31.85	4.31	4.55	10.41	1.6	28.51	0.85	1.42	8.89	—

Table 4. Sr-8 SEM point element distribution (mass fraction, %).

Element	w(C)	w(O)	w(Mg)	w(Al)	w(Si)	w(P)	w(Ca)	w(S)	w(V)	w(Cr)	w(Ti)	w(Mn)	w(Fe)	w(Br)
Point 5	2.65	38.93	13.26	20.38	0.02	0	0.44	—	—	1.1	—	3.28	19.94	—
Point 6	3.05	34.68	0.37	2.41	3.04	0.04	27.8	—	—	—	8.89	1.98	17.73	—
Point 7	9.53	35.25	0.18	0.00	11.86	1.69	37.03	—	1.25	—	—	0.29	1.09	1.84
Point 8	41.47	22.24	0.1	0.73	7.15	1.07	24.19	0.36	0.65	—	0.49	0.28	1.27	—

Table 5. Sr-12 SEM point element distribution (mass fraction, %).

Element	w(C)	w(O)	w(Mg)	w(Al)	w(Si)	w(P)	w(Ca)	w(Ti)	w(Mn)	w(Fe)
Point 9	4.81	43.94	0.24	3.11	3.39	0.02	23.74	7.35	1.62	11.8
Point 10	3.67	41.64	0.25	15.26	9.28	0.06	25.04	—	0.16	4.65
Point 11	3.20	33.02	0.25	1.78	2.74	0.00	29.68	9.62	1.67	18.02
Point 12	7.67	31.89	3.42	3.07	9.06	0.69	19.72	—	4.90	19.57

From the surface scan and energy spectrum shown in Figure 4, combined with the elemental distribution shown in Table 4, it is suggested that point 5 had the same physical

phase as point 1, i.e., MFA. At point 6, the $n(\text{CaO}):n(\text{Fe}_2\text{O}_3)$ ratio was 2:1. Additionally, the Ti content in the experimental slag was reduced, while the percentage share in the test was higher, considering the identification problem; therefore Ti was not considered as a factor at this stage, and the material phase at point 6 was considered to be dicalcium ferrate ($2\text{CaO}\cdot\text{Fe}_2\text{O}_3$, C_2F). The physical phases at points 7 and 8 were the same as those at point 2, i.e., silicate phases with phosphorus attached. The C content in the point sweep elements was high, possibly due to the use of a polishing agent; the main components of the polishing agent used were diamond micropowder and grinding media. As such, polishing agent residue on the surface of the specimen likely resulted in the high carbon content observed in the distribution of elements, especially around the hole residue, such as at point 8, where the carbon content was 41.47%. The detection of carbon was not further explored at this stage of our research.

The surface scan and energy spectrum shown in Figure 5, combined with the analysis of elemental distribution shown in Table 5, suggest that points 9, 11, and 12 had the same phase as point 6, i.e., C_2F ; the main phase at point 10 was calcium aluminum yellow feldspar ($\text{Ca}_2\text{Al}_2\text{SiO}_7$, C_2AS).

In summary, the scanning electron microscopy data complemented the XRD results. The phases contained in the steel slag, as determined via SEM-EDS, were MFA, a magnesium-iron phase solid solution with a low melting point, $\text{Ca}_3(\text{PO}_4)_2$ and CaSiO_3 (in an elliptical shape), C_2F (with a milky white color), and C_2AS (with a light gray color and hexagonal shape). C_2AS and C_2F formed a molten structure, and with the increase of blast furnace slag doping, the percentage of C_2AS in the physical phase increased, causing significant cracks to appear in S_r -12. This shows that with an increase of the blast furnace slag doping ratio, the alkalinity of tempered slag decreases, which is conducive to the generation of C_2S and the crystalline transformation of some C_2S from β - C_2S to γ - C_2S , which expands to about 11% in volume. Additionally, the internal stresses resulted in the appearance of fine cracks inside the slag. On the other hand, the proportion of Al_2O_3 in blast furnace slag is relatively high, and the increase of its content promotes the generation of C_2AS in tempered slag.

In order to further determine its macroscopic structure, the tempered slag was photographed using $300\times$ and $500\times$ lenses on a mineralogical microscope; see Figure 6. As shown, S_r -0 and S_r -10 were selected as the C_2AS material phase fraction. It was observed that with an increase of blast furnace slag doping, the quantity of C_2AS with a hexagonal shape in the material phase was reduced and black triangular forms appeared in the middle part. This indicated that the doping of blast furnace slag had a grain refining effect on C_2AS . The S_r -8 calcium ferrate and silicate became interwoven, forming more needle-like calcium ferrate phase. Because needle-like calcium carbonate has high strength, an increase of its content can increase the strength of slag, indirectly increasing the cost of steel slag crushing. As shown in S_r -12 and S_r -15, silicate, calcium ironate, and calcium alumina yellow feldspar were present in relatively similar abundances. From Figure S_r -12 and S_r -15, it can be seen that the proportion of hexagonal calcium alumina yellow feldspar had decreased significantly, forming a smaller volume of calcium alumina yellow feldspar and wrapped by silicate. Additionally, the content of needle-like calcium ironate decreased significantly while that of silicate increased significantly. This was in accordance with the XRD diffraction pattern, which showed that the intensity of silicate (C_3S) diffraction was enhanced with an increase in the blast furnace slag doping ratio.

In summary, on the one hand, blast furnace slag high-temperature molten tempered steel slag can refine the grain of calcium aluminum yellow feldspar, reduce the content of needle-like calcium ferrate, and indirectly reduce the cost of steel slag crushing. On the other hand, blast furnace slag blending can reduce the alkalinity of steel slag and promote the generation of a silicate phase with high hydration activity, providing a reference for the blending of steel slag in cement concrete.

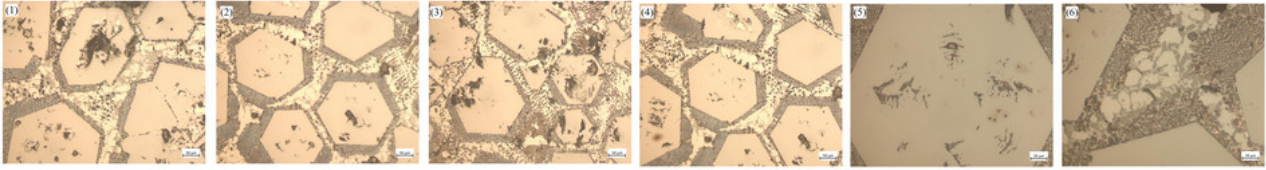
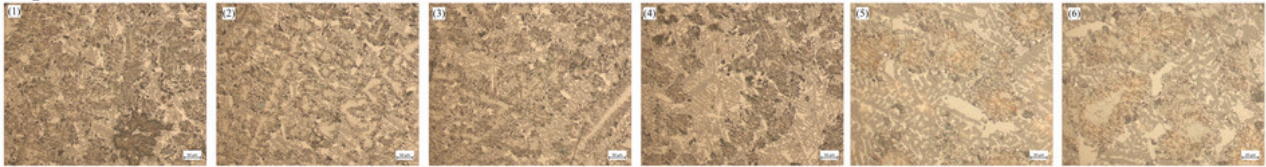
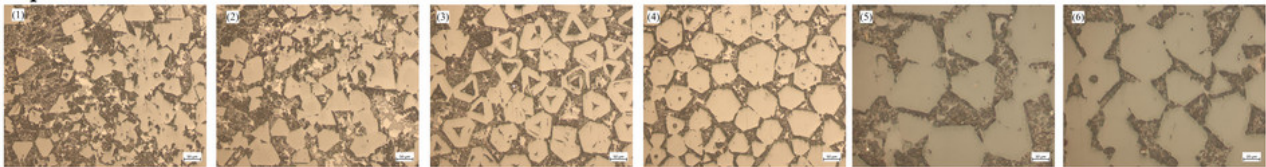
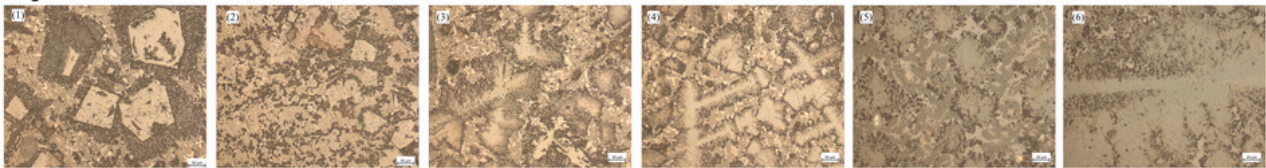
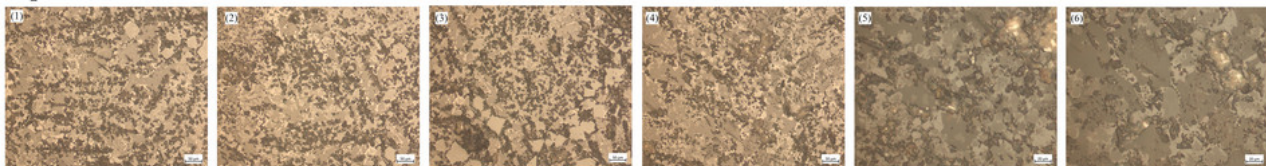
S_r-0**S_r-8****S_r-10****S_r-12****S_r-15**

Figure 6. Mineralogram of blast furnace slag tempered slag roasting specimen. (1) to (4) are 300× magnified mineral phases, (5) and (6) are 500× magnified mineral phases.

3.3. Modified Slag FactSage7.1 Calculation Results and Analysis

In order to further determine the phase composition of the modified steel slag, the equilibrium phase composition of 100 g of tempered slag was simulated using the equilibrium module in the FactSage7.1 thermodynamic calculation software; the results are shown in Figure 7. As shown, in the low temperature section (1000 °C–1250 °C), an increase of blast furnace slag doping results in greater inhibition of the generation of C_2S , $a-C_2S-C_3P$, and C_2F and promotes the generation of magnesia rose pyroxene ($Ca_3MgSi_2O_8$, C_3MS_2) and dicalcium aluminate ($Ca_2Al_2O_5$, C_2A). Our analysis suggests that when the temperature is lower than 1250 °C, P_2O_5 is very easy to solid-solve in C_2S to form $a-C_2S-C_3P$, which consumes a large amount of C_2S and causes the C_2S content to decrease sharply at 1000 °C–1250 °C. According to existing research, P_2O_5 solid solution in C_2S can inhibit the crystalline transformation of C_2S from $\beta-C_2S$ to $\gamma-C_2S$ and improve the stability of steel slag. The alkalinity of blast furnace slag is about 1.0; it usually contains 13.92% Al_2O_3 and 8.26% MgO . With an increase of the blast furnace slag doping ratio, the Al_2O_3 and MgO contents in the slag after tempering increase, and the binary alkalinity decreases. The generation of C_3MS_2 and C_2A in the low temperature section consumes some of the Ca^{2+} ions and indirectly inhibits the generation of C_2S and $Ca_2Fe_2O_5$, as C_3MS_2 and C_2A are low

melting point minerals. When the temperature is higher than 1250 °C, $\text{Ca}_2\text{Fe}_2\text{O}_5$ and C_2A partially melt and C_3MS_2 completely melts. All compounds enter the liquid phase when the temperature is higher than 1350 °C, thereby enriching the Ca^{2+} and Si^{4+} ions in the liquid phase. As shown in Figure 7a, the C_2S content in the tempered slag mixed with blast furnace slag increased at a higher rate than that in the steel slag without blast furnace slag at temperatures from 1250 °C to 1450 °C, and the C_2S content in the equilibrium phase increased gradually as the temperature increased. The C_2S content reached a maximum at a temperature of 1400 °C. The steel slag was tempered with 15% blast furnace slag and the C_2S content reached 39.04 g. The C_2S content in the slag at this temperature was only 16.92 g, i.e., only 1/4 that of the S_r -15 tempered slag. From Figure 7c, it can be seen that S_r -8, S_r -10, and S_r -12 started to enter the liquid phase at 1350 °C, and the amount of liquid phase increased with an increase in the ration of blast furnace slag doping. Our analysis indicated that the steel slag which was not mixed with blast furnace slag did not generate C_3MS_2 in the low-temperature section, and as such, as the temperature increased to 1350 °C, no low-melting point material melted. Combined with the data shown in Figure 7b), it was found that S_r -0 did not melt at 1350 °C, and therefore, no liquid phase was generated in S_r -0 at that temperature. S_r -15 did not produce a liquid phase at 1350 °C. Our analysis suggests that the liquid phase produced by the melting of C_3MS_2 and $\text{Ca}_2\text{Fe}_2\text{O}_5$ at 1350 °C rapidly generated C_2S with SiO_2 in the steel slag, but, given that the melting temperature of C_2S is high, a liquid phase was not reached at 1350 °C. A liquid phase environment can promote exchanges among ions and accelerate reactions. However, a large amount of dopant was shown to produce more non-gelatinized C_2AS . Therefore, it was concluded that 12% dopant content is optimal. As shown in Figure 7g, the doping of blast furnace slag has an inhibitory effect on the formation of $\text{Ca}_7\text{P}_2\text{Si}_2\text{O}_{16}$ at temperatures ranging from 1000 °C to 1045 °C. At temperatures above 1050 °C, S_r -0~ S_r -12 melted into the liquid phase, while S_r -15 slowly entered the liquid phase as the temperature increased. As shown in Figure 7e), the doping of blast furnace slag can indirectly inhibit the generation of $\text{a-C}_2\text{S-C}_3\text{P}$. At a temperature of 1300 °C, the $\text{a-C}_2\text{S-C}_3\text{P}$ content in the slag not containing blast furnace slag was maximal, i.e., 37.67 g, while the $\text{a-C}_2\text{S-C}_3\text{P}$ content in the slag tempered with 12% blast furnace slag was only 18.82 g. With an increase in temperature, the $\text{a-C}_2\text{S-C}_3\text{P}$ content decreased rapidly. A temperature higher than 1350 °C is required to reach the melting point of $\text{a-C}_2\text{S-C}_3\text{P}$. As such, experiments had to be carried out at above 1450 °C. A comparison of our analysis compared with the experimental scan results showed that the roasted tempered slag contained a significant amount of C_2AS . We concluded that the thermodynamic calculations yielded results for the equilibrium phase in the ideal state, while the experimental environment could not reach an ideal state, and the C_2A generated by the tempered slag reacted with the SiO_2 in the slag to produce C_2AS minerals. This also explains the presence of the silicate phase in the form of CaSiO_3 in the roasted specimens. In order to achieve the state described in the thermodynamic calculations, it would be necessary to increase the roasting temperature, extend the holding time, improve the liquid phase fluidity of the slag, improve the high temperature kinetic conditions of the slag, and enhance the electromagnetic stirring, gas stirring, or other stirring methods.

In summary, the doping of blast furnace slag can promote the generation of low melting point minerals such as C_3MS_2 and C_2A , provide a liquid phase for the low temperature section of the tempering slag, improve the low temperature kinetic characteristics of the tempering slag, and promote the generation of C_2S , making it possible to calculate the amount of liquid phase in the high temperature section at a roasting temperature of around 1550 °C. Blast furnace slag tempering slag, on the one hand, promotes the generation of low melting point minerals, improves the low temperature kinetic characteristics of the slag, promotes the generation of C_2S , inhibits the generation of high strength minerals such as calcium ferrate, and reduces the strength of the slag, thereby indirectly reducing the cost of crushing. On the other hand, blast furnace slag doping can inhibit the generation of $\text{a-C}_2\text{S-C}_3\text{P}$, and, according to existing research, can result in the enrichment of P_2O_5 ,

which has a strong inhibitory effect on the crystalline transformation of C_2S . Therefore, reducing the content of $a-C_2S-C_3P$ in a self-powdering steel slag is advantageous.

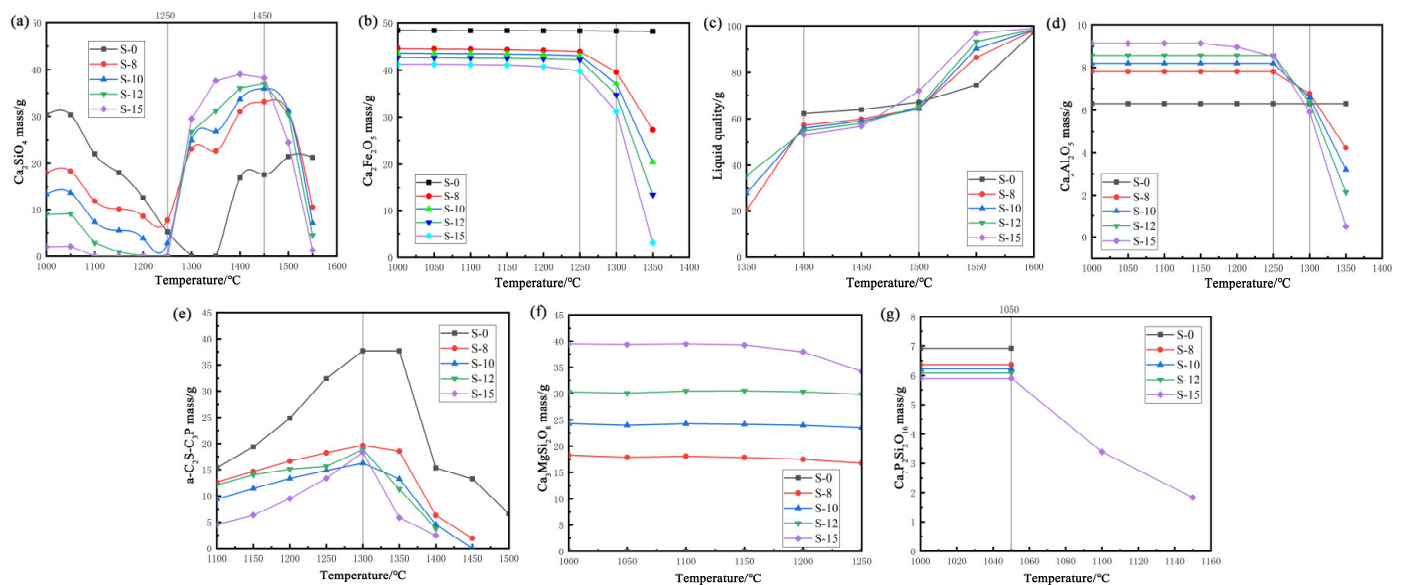


Figure 7. Equilibrium phase composition of tempered slag. (a–g) are the masses of Ca_2SiO_4 , $Ca_2Fe_2O_5$, liquid quantity, $Ca_2Al_2O_5$, $a-C_2S-C_3P$, $Ca_3MgSi_2O_8$, and $Ca_7P_2Si_2O_{16}$ in the material phase at equilibrium, respectively.

4. Conclusions

- (1) In blast furnace slag tempering steel slag, the blast furnace slag doping mass fraction should be about 12% or less in order to promote the generation of minerals with gelling activity such as C_3S , to indirectly consume the f -CaO present in the steel slag, to improve the stability, to limit the abundance of non-gelling C_2AS , and to achieve higher hardness via C_3AS_3 mineral generation, thereby reducing the cost of steel slag crushing.
- (2) As shown in the SEM-EDS data, the phases contained in the steel slag were MFA, a magnesium-iron phase solid solution with a low melting point, $Ca_3(PO_4)_2$ and $CaSiO_3$ (with elliptical shape), C_2F (with a milky white color), and C_2AS (with a light gray color and hexagonal shape). Blast furnace slag doping, on the one hand, can refine the grain of calcium aluminum feldspar and reduce the content of acicular calcium ferrate in the tempered slag. On the other hand, it can reduce the alkalinity of the slag and promote the generation of a silicate phase with high hydration activity.
- (3) Thermodynamic calculations showed that doping blast furnace slag promotes the generation of low melting point minerals (notably C_3MS_2 and C_2A), provides a liquid phase for the low temperature section ($1000\text{ }^\circ\text{C}\sim 1250\text{ }^\circ\text{C}$), improves the low temperature kinetic characteristics of the tempered slag, promotes the generation of C_2S in the high temperature section ($1250\text{ }^\circ\text{C}\sim 1600\text{ }^\circ\text{C}$), inhibits the generation of $a-C_2S-C_3P$ and calcium ferrate minerals, and reduces the strength of steel slag.

Author Contributions: Conceptualization, S.H. and G.L.; methodology, S.H.; software, Y.L.; validation, Y.C., G.L. and W.S.; formal analysis, G.L.; investigation, S.H.; resources, S.H.; data curation, S.H.; writing—original draft preparation, S.H.; writing—review and editing, S.H.; visualization, G.L.; supervision, S.A.; project administration, G.L.; funding acquisition, G.L. All authors have read and agreed to the published version of the manuscript.

Funding: National Key R&D Program funded project (2020YFC1909105); Inner Mongolia Autonomous Region Science and Technology Major Special Project (2021ZD0016-05-04).

Data Availability Statement: All authors can confirm that all data used in this article are available for publication.

Conflicts of Interest: No conflict of interest exists in the submission of this manuscript, and the manuscript is approved by all authors for publication.

References

1. Ibrahim, S.; Meawad, A. Towards green concrete: Study the role of waste glass powder on cement/superplasticizer compatibility. *J. Build. Eng.* **2022**, *47*, 103751. [[CrossRef](#)]
2. Anandaraj, S.; Karthik, S.; Vijaymohan, S.; Rampradheep, G.S.; Indhiradevi, P.; Anusha, G. Effects of using white flour, zinc oxide and zinc ash as an admixture in mortar and concrete. *Mater. Today Proc.* **2022**, *52*, 1788–1793. [[CrossRef](#)]
3. Cheng, X.; Tian, W.; Gao, J.F.; Gao, P. Performance evaluation and lifetime prediction of steel slag coarse aggregate concrete under sulfate attack. *Constr. Build. Mater.* **2022**, *344*, 128203. [[CrossRef](#)]
4. Du, X.Q.; Huang, Z.; Ding, Y.; Xu, W.; Zhang, M.; Wei, L.B.; Yang, H.R. Feasibility Study of Grinding Circulating Fluidized Bed Ash as Cement Admixture. *Materials* **2022**, *15*, 5610. [[CrossRef](#)]
5. Long, H.; Huang, X.Y.; Liu, M.J.; Cui, C.H.; Li, L.; Liao, Y.; Yan, D.H. The fate of heavy metals in the co-processing of solid waste in converter steelmaking. *J. Environ. Manag.* **2022**, *311*, 114877. [[CrossRef](#)] [[PubMed](#)]
6. Liu, G.; Schollbach, K.; Li, P.P.; Brouwers, H.J.H. Valorization of converter steel slag into eco-friendly ultra-high performance concrete by ambient CO₂ pre-treatment. *Constr. Build. Mater.* **2021**, *280*, 122580. [[CrossRef](#)]
7. Yong, Y.; Shaopeng, W.; Chao, L.; Dezhi, K.; Benan, S. Morphological Discrepancy of Various Basic Oxygen Furnace Steel Slags and Road Performance of Corresponding Asphalt Mixtures. *Materials* **2019**, *12*, 2322. [[CrossRef](#)] [[PubMed](#)]
8. Yee, C.L. Reutilization of dredged harbor sediment and steel slag by sintering as lightweight aggregate. *Process Saf. Environ. Prot.* **2019**, *126*, 287–296.
9. Wang, L.; Wu, L.B.; Tang, Y.; Wang, B.H.; Sun, K.; Ishimwe, A. Liquefaction resistance behaviours of gravel steel slag. *Eur. J. Environ. Civ. Eng.* **2022**, *26*, 4643–4663. [[CrossRef](#)]
10. Wang, Q.; Long, J.F.; Xu, L.L.; Zhang, Z.; Lv, Y.; Yang, Z.H.; Wu, K. Experimental and modelling study on the deterioration of stabilized soft soil subjected to sulfate attack. *Constr. Build. Mater.* **2022**, *346*, 128436. [[CrossRef](#)]
11. Ju, J.R.; Feng, Y.L.; Li, H.R.; Xu, C.L.; Yang, Y. Efficient Separation and Recovery of Vanadium, Titanium, Iron, Magnesium, and Synthesizing Anhydrite from Steel Slag. *Min. Metall. Explor.* **2022**, *39*, 733–748. [[CrossRef](#)]
12. Ju, J.R.; Feng, Y.L.; Li, H.R.; Xu, C.L.; Yang, Y. Research progress and prospect of steel slag modification. *Environ. Eng.* **2020**, *39*, 136–140.
13. Zhang, X. *Carbonation Mechanism of Steel Slag Products Modified by Zeolite*; Dalian University of Technology: Dalian, China, 2021.
14. Xiang, R.H. *Study on Preparation and Foaming Modification of Reconstituted Steel Slag Powder with Medium and High Activity*; Guilin University of Technology: Guilin, China, 2021.
15. Rao, L. *Study on Internal Law of Composition, Structure and Properties of Converter Steel Slag and Its Application*; University of Science and Technology Beijing: Beijing, China, 2020.
16. Wang, C.L.; Zhao, G.F.; Wang, Y.B.; Zhang, S.H.; Zheng, Y.C.; Huo, Z.K.; Wang, Z.X.; Ren, Z.Z.; Zhou, J.Y. High temperature modification of steel slag from reservoir sediment and calcium carbide slag. *Mater. Rev.* **2022**, *36*, 127–133.
17. Zaibo, L.; Sanyin, Z.; Xuguang, Z.; Tusheng, H. Cementitious property modification of basic oxygen furnace steel slag. *Constr. Build. Mater.* **2013**, *48*, 575–579.
18. Zhang, Z.S.; Lian, F.; Liao, H.Q.; Yang, Q.; Cao, W.B. Properties of steel slag modified by iron tailings at high temperature. *J. Univ. Sci. Technol. Beijing* **2012**, *34*, 1379–1384.
19. Lei, Y.B.; Zhang, Y.Z.; Xing, H.W.; Long, Y.; Tian, T.L. High temperature Melting and digestion of free CaO from converter slag mixed with fly ash. *Hebei Metall.* **2011**, *4*, 11–14.
20. Liu, S.Y.; Wang, Z.J.; Peng, B.; Yue, C.S.; Guo, M. Physical and chemical basis of steel slag modified by blast furnace slag. *J. Eng. Sci.* **2018**, *40*, 557–564.
21. Zhang, W.; Hao, X.S.; We, C.; Liu, X.M.; Zhang, Z.Q. Activation of low-activity calcium silicate in converter steelmaking slag based on synergy of multiple solid wastes in cementitious material. *Constr. Build. Mater.* **2022**, *351*, 128925. [[CrossRef](#)]
22. Niu, F.; An, Y.; Zhang, J.; Chen, W.; He, S. Synergistic Excitation Mechanism of CaO-SiO₂-Al₂O₃-SO₃ Quaternary Active Cementitious System. *Front. Mater.* **2021**, *8*, 792682. [[CrossRef](#)]

Disclaimer/Publisher's Note: The statements, opinions and data contained in all publications are solely those of the individual author(s) and contributor(s) and not of MDPI and/or the editor(s). MDPI and/or the editor(s) disclaim responsibility for any injury to people or property resulting from any ideas, methods, instructions or products referred to in the content.